The Penetration of Mountain Waves into the Middle Atmosphere*

MARK R. SCHOEBERL

Laboratory for Atmospheres, Code 616, NASA/Goddard Space Flight Center, Greenbelt, MD 20771

(6 March 1985 and 9 August 1985)

ABSTRACT

A linear nonhydrostatic model of gravity waves forced by a bell-shaped ridge is used to investigate the penetration of mountain waves into the stratosphere and mesosphere during winter and fall. Gravity waves with horizontal scales less than 30 km are found to be trapped near the tropopause and the stratopause in regions of strong winds. The effect of trapping these modes produces a disturbance whose structure broadens with height. In the mesosphere the disturbance appears 20–40 km downstream from the forcing depending on the strength of the intervening winds.

Wavebreaking associated with the mountain wave is predicted in the lower stratosphere as a result of wave superposition; no individual harmonic reaches breaking amplitude. In the mesosphere, wave breakdown is more prevalent, and the disturbance spectrum is relatively more monochromatic as a result of the filtering of the shorter scale modes by the lower atmosphere.

1. Introduction

Mountain waves are small-scale stationary gravity waves forced by flow over topography. The first comprehensive mathematical treatment of these waves for tropospheric flows was made by Scorer (1949), Queney (1947), and Queney *et al.* (1960). They showed that gravity waves with horizontal scales less than about 20 km are trapped by the low stability and strong winds in the upper troposphere. Thus, a gravity wave forced by flow over a small ridge propagates vertically, is reflected, returns to the surface, is reflected again, etc., leaving a stationary wave train downstream of the ridge. The manifestation of this lee wave train is often a periodic line of clouds which forms where the upward vertical displacement due to the wave is large.

While mountain waves and other types of gravity waves can have important local effects on the flow, they probably play only a secondary role in the general circulation of the troposphere.[1] In the mesosphere, on the other hand, gravity waves are a fundamental ingredient in the general circulation. This condition exists because gravity waves originating in the troposphere reach very large amplitudes in the mesosphere. The breakdown of these gravity waves places a stress on the flow, accelerating it toward the phase speed of the gravity wave. It is this acceleration which is believed to provide the closure of the stratospheric solstitial jets in the mesosphere (Lindzen, 1981; Matsuno, 1982).

In order to better understand the mesospheric circulation, it is important to understand the tropospheric sources of gravity waves and their propagation properties through the intervening layers. Obviously, topography is one of the richest sources of stationary gravity waves. Although in his seminal paper, Lindzen (1981) considered gravity waves with horizontal scales on the order of 1000 km, recent observational results from Vincent and Reid (1983) and others suggest that gravity waves which provide the greatest momentum input to the mesosphere have scales shorter than 100 km. It is possible that these waves are the remnants of mountain waves. The forcing and propagation of mountain waves into the mesosphere is the subject of this investigation.

For typical tropospheric flows, waves with horizontal scales of 30 km or greater can be considered nearly hydrostatic (Klemp and Lilly, 1980). However, in the stratospheric jets, the intrinsic frequency of stationary gravity waves with a 30 km scale approaches the local buoyancy frequency. Under such conditions, the wave is internally reflected, a process which takes place in a finite time (Bretherton, 1969). Gravity waves modeled using the hydrostatic assumption, on the other hand, experience internal reflection only in the presence of strong shears or sharp density gradients. Therefore, for waves with scales on the order of 30–50 km, important differences between hydrostatic and nonhydrostatic middle atmosphere gravity wave models will exist.

To study the propagation of mountain waves in the

* Contribution No. 24 of the Stratosphere General Circulation with Chemistry Project, NASA/GSFC.

[1] This is not to say they are unimportant. As Lilly (1972) pointed out, the neglect of the drag on the troposphere by small scale features could be one reason for error in long range forecasts. This idea has more or less been confirmed with general circulation model studies (Boer *et al.*, 1984; Palmer, private communication, 1984).

mesosphere, we use a two-dimensional, linear, nonhydrostatic model with periodic zonal boundaries. This model is chosen for a number of reasons. First, it is computationally inexpensive to run at very high resolution, and therefore allows a number of relatively realistic experiments to be performed. Second, the linear theory of nonhydrostatic waves is well understood, and results of the model can be checked with previous work. Finally, a radiation condition at the upper boundary is easily formulated.

There are also some disadvantages in using this type of model. First, the periodic lateral boundary conditions sometimes make it difficult to separate upstream and downstream effects. However, ray tracing computations are also presented which will help clarify these processes. Second, wavebreaking effects feeding back on the wave and the mean flow cannot be self-consistently incorporated in this model. To overcome this problem the topographic forcing is adjusted to minimize the predicted regions of instability in the stratosphere so that the assumption of a stationary wave and mean flow is reasonably justified. Finally, the neglect of nonlinear effects could have a significant impact on our results. A comparison of linear versus nonlinear models of hydrostatic mountain waves by Klemp and Lilly (1978) indicated that nonlinear effects tended to increase the pressure gradients associated with mountain waves where those gradients were already strong in the linear model. Otherwise the linear model appeared to do a good job of reproducing the structure of the mountain wave up to the lower stratosphere. Since we are already minimizing the wave amplitudes in the stratosphere, nonlinear effects will be unimportant.

In section 2 the model and relevant equations are discussed. For those unfamiliar with the dynamics of mountain waves, Gill (1982; pgs. 274–294) and Smith (1979) provide excellent, comprehensive reviews and bibliographies. Section 3 shows our results for two representative basic flow states. The conclusions are presented in section 4.

2. Model

a. Equations

Klemp and Lilly (1980) derived the relevant equation for linear nonhydrostatic gravity waves; the derivations will not be repeated here. These equations are valid under the anelastic approximation of Ogura and Phillips (1962). This approximation is derived assuming a constant basic state potential temperature; however, for a model which extends to the mesosphere such assumption is inappropriate. Nevertheless, the correction to the wave amplitude due to increasing potential temperature with height is small and can be neglected for our purposes.

If the vertical velocity w' is Fourier decomposed in the x direction and density weighted so that

$$w'(x, z) = w(z)e^{ikx+z/2H}$$

where z is height and k the zonal wavenumber, then in the absence of rotation, the gravity wave vertical structure is determined by the solution of

$$w_{zz} + \left\{\frac{N^2}{\bar{u}^2} - \frac{\bar{u}_{zz}}{\bar{u}} - \frac{\bar{u}_z}{\bar{u}H} - \frac{1}{4H^2} - k^2\right\}w = 0, \quad (1)$$

where the subscript denotes differentiation with respect to height. The buoyancy frequency is denoted by N, H is the local scale height (assumed to vary weakly with z) and $\bar{u}$ is the zonal wind; the overbar represents zonal averaging. For reference we define the Scorer parameter,

$$S^2 = \frac{N^2}{\bar{u}^2} - \frac{\bar{u}_{zz}}{\bar{u}} - \frac{\bar{u}_z}{H\bar{u}} - \frac{1}{4H^2}.$$

In the case of hydrostatic gravity waves, (1) is simply

$$w_{zz} + S^2 w = 0. \quad (2)$$

Comparing (1) and (2) it is clear that hydrostatic waves become evanescent only when S^2 becomes negative, which will occur only in regions of unusually strong curvature or shear in the zonal wind. For usual atmospheric flows S^2 is positive. Nonhydrostatic waves become evanescent when $S^2 - k^2$ becomes negative, which is easily accomplished for waves with small horizontal scale.

A gravity wave which propagates vertically from some forcing region and becomes evanescent due to sign change in $S^2 - k^2$ is reflected (Bretherton, 1969). In a steady state model, the internal reflection of forced gravity waves can lead to resonance. That is, modes which form standing waves due to the reflection and have a node close to the surface where the wave is forced can achieve extreme amplitudes.

In the real atmosphere, resonance may be more difficult to achieve than in a steady state model. Using (1), the group velocities are given by

$$C_{gx} = \frac{k^2\bar{u}^3}{N^2}, \quad (3a)$$

$$C_{gz} = \pm\frac{k\bar{u}^2}{N}\left(1 - \frac{k^2\bar{u}^2}{N^2}\right)^{1/2}. \quad (3b)$$

The vertical group velocity is either upward or downward depending on the vertical phase tilt of the wave. However, the horizontal group velocity is always downstream. (Note that in the hydrostatic case the horizontal group velocity for this problem is zero.) Thus, a disturbance generated by some topographic feature while propagating vertically to its reflection level will also be advected downstream. After reflection it will then return to the surface downwind of the original forcing to be reflected back into the upper atmosphere. If there is no forcing at the downstream surface reflection point, the wave cannot pick up more energy for resonance. Thus, because of the periodic lateral

boundaries which will always return the wave to the forcing region, this model will be more sensitive to resonance.

b. Numerical model

Because the numerical model must extend to the mesosphere and the vertical wavelength of gravity waves in weak wind regions can be very small, a large number of grid points is required. The minimum resolution needed to produce nearly invariant solutions was determined experimentally to be ¼ km vertically and 1 km horizontally for the mountain widths discussed below. A domain of 200 km wide extending to 80 km is used. Equation (1) is solved for each harmonic, k; then the result is Fourier synthesized to determine the total solution.

The upper boundary is placed at 80 km and the radiation condition

$$\frac{\partial w}{\partial z} = i\gamma w$$

is imposed where,

$$\left.\begin{aligned}\gamma &= (S^2 - k^2)^{1/2}, S^2 > k^2\\ \gamma &= i(k^2 - S^2)^{1/2}, S^2 < k^2\end{aligned}\right\}.$$

This condition guarantees that waves are not reflected from the upper boundary. As an independent check, a computation of the reflection coefficient for each propagating mode at the upper boundary has been made, and the radiation condition was satisfied.

Lower boundary forcing is produced by a bell shaped mountain ridge whose height is given by

$$h(x) = \frac{h_0 a^2}{(a^2 + x^2)}$$

where a is the equivalent mountain half-width. The vertical velocity produced by flow over the mountain is given by

$$w = ik\bar{u}\bar{h}(k),$$

where $\bar{h}(k)$ is the Fourier transform of $\bar{h}(x)$,

$$\bar{h}(k) = \pi h_0 a e^{-ak}.$$

With this type of forcing, the peak in the w' spectrum occurs at $k = a^{-1}$. Experiments were performed with a variety of mountain widths (1, 2, 4, 8 km); however, for brevity only the 4 km width results will be shown in section 3. All of the computations using different mountain widths gave results consistent with shifting the peak in the forcing spectrum.

The use of a bell-shaped ridge tends to overforce gravity waves since the air is constrained to go over the mountain. In the case of a small isolated mountain, air is more likely to flow around the mountain producing little gravity wave forcing. Even in the presence of a substantial mountain range, air may initially flow over the mountains until upstream dynamics alter the flow to bring air around the range (Pierrehumbert and Wyman, 1985). This kind of flow change may take place in less than one day. Thus mountain wave forcing, in reality, can be both highly time dependent and very nonlinear.

c. Basic state

Two zonal wind profiles representing winter solstice and fall equinox were used as the basic state. These profiles are shown in Fig. 1. The static stability was computed from a smoothed version of the 1962 U.S. Standard Atmosphere. The winter profile is based on zonal wind cross section at 35°N taken from the four year average for December published by Wu *et al.* (1985). The equinoctial wind profile is based on an October zonal wind cross section at 45°N from the same source. Since spring and summer zonal wind profiles usually have critical lines for stationary waves in the stratosphere, they were not considered. Propagation of mountain waves into the mesosphere under such conditions would be forbidden.

In all of the computations, the effects of radiative damping were included. For radiative damping, the wavenumber dependent scheme of Fels (1982) was used by approximating the vertical wavenumber γ as

$$\gamma = |S^2 - k^2|^{1/2}.$$

The effects of rotation were also tested and were found to be unimportant for the wind profiles shown in Fig. 1.

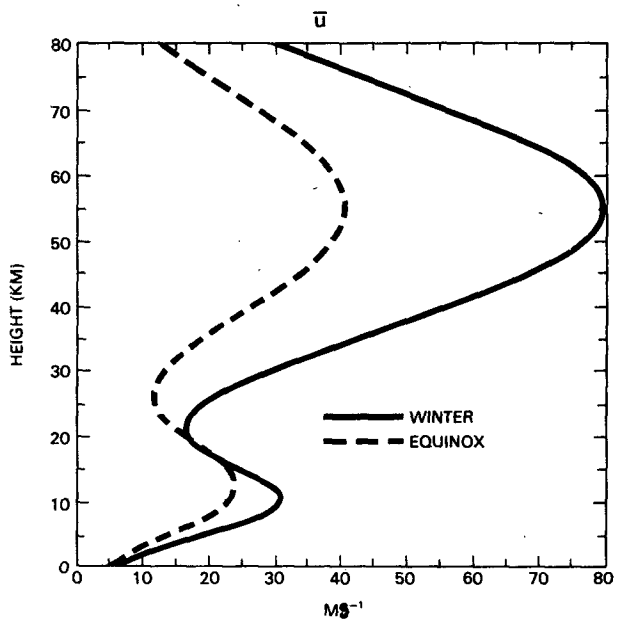

FIG. 1. The zonal wind profiles used as the basic state are shown. The winter and equinox winds were estimated from the monthly mean zonal winds from Wu *et al.* (1985).

3. Results

a. Solutions to gravity wave equation

As previously mentioned, once the steady state solution is obtained for a certain mountain height, the result is checked for regions where the Richardson number is less than one-quarter in the stratosphere. Gravity wave breakdown would normally occur in that region resulting in dissipation of the wave and strong vertical momentum flux convergence. Under such conditions the basic state would be altered so that the steady solution would no longer be valid. The mountain height is therefore adjusted and the computation repeated until the low Richardson number region in the stratosphere is reduced to a minimal size. For mountains with 4 km width using the winter wind profile, heights below 0.6 km produced unstable solutions only in the mesosphere.

Figure 2 shows the computed displacements for 4 km wide mountains for the winter and equinox profiles shown in Fig. 1. The displacement η is defined as

$$\eta = w'(\bar{u}k)^{-1}$$

which, for a linear model, is also the streamline. The displacement is drawn with the same scale as the ordinate so that the displacement from the surface follows the mountain topography. The shaded regions in each figure locate roughly where the Richardson number is less than one-fourth; zones where gravity wave breakdown might be expected.

It is immediately apparent from Fig. 2 that wave breaking zones exist in the stratosphere for both wind profiles. In the troposphere, the disturbance is localized over the topography, but above the troposphere the width of the disturbance broadens in scale with altitude. In the mesosphere, wavebreaking is predicted over an extensive horizontal region.

To understand the results shown in Fig. 2, the horizontal wavelength of each mode is plotted as a vertical line against $2\pi/S$, the Scorer wavelength, in Fig. 3. The $2\pi/S$ line divides the wave propagation region from the evanescent region, and the intersection, a wavelength line with $2\pi/S$, shows where each mode is internally reflected. From Fig. 3 it is apparent that two zones of reflection exist; one just below the tropopause at about 10 km, and one just at and below the stratopause at 50 km. These regions occur where the strong winds push the gravity wave intrinsic frequency ($k\bar{u}$) toward the buoyancy frequency. The tropopause jet traps most of the gravity waves with scales smaller than 10–15 km. It is the absence of these smaller-scale waves in the stratosphere which causes the disturbance above the tropopause to broaden with height. Waves with scales less than 15–30 km are trapped below the stratopause so that the disturbance broadens even further at mesospheric altitudes. The comparative trapping of more small-scale waves by the winter wind profile directly leads to the greater broadening of the disturbance with altitude compared with the equinox solution.

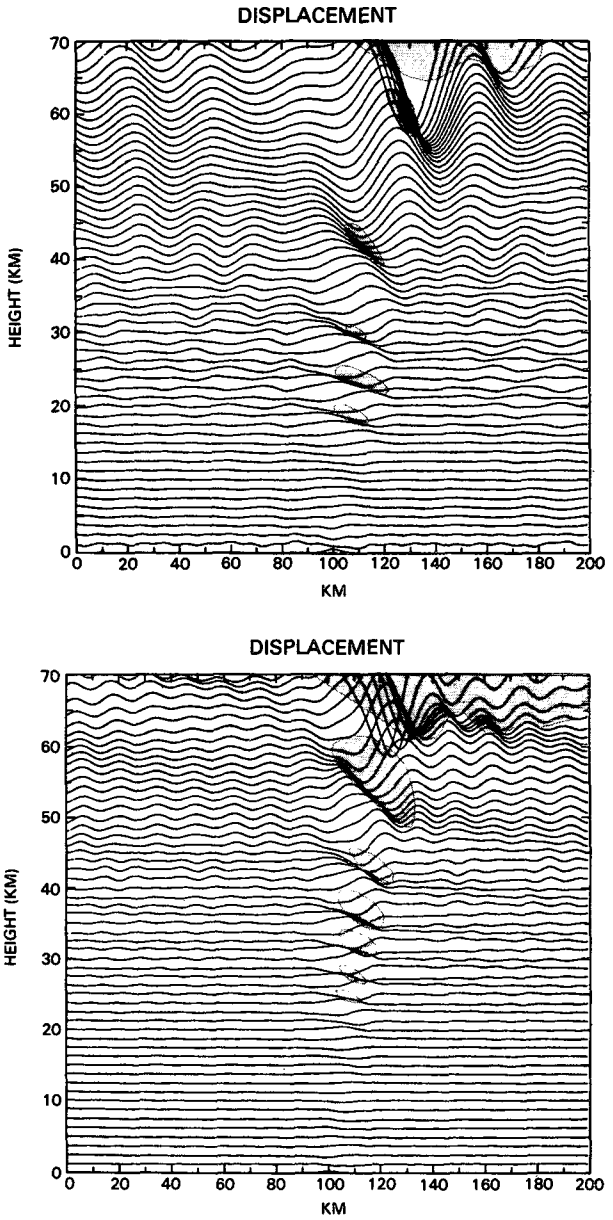

FIG. 2. Particle displacements associated with mountain waves are shown at different altitudes. The mountain is centered at 100 km and is profiled by the lowest displacement line. Panel (a), shows results using the winter wind profile; panel (b), the equinox wind profile. Shaded regions indicate zones where Ri < 1/4.

To illustrate the two wave trapping regions in another way, Fig. 4 shows the ray paths for individual wave packets of the larger horizontal scale modes. The ray paths are computed assuming that when a reflection region or the ground is encountered the wave is totally reflected. [This procedure is used only for illustration. Since reflection of the wave results from a turning point in (1), the slowly varying phase approximation (WKB

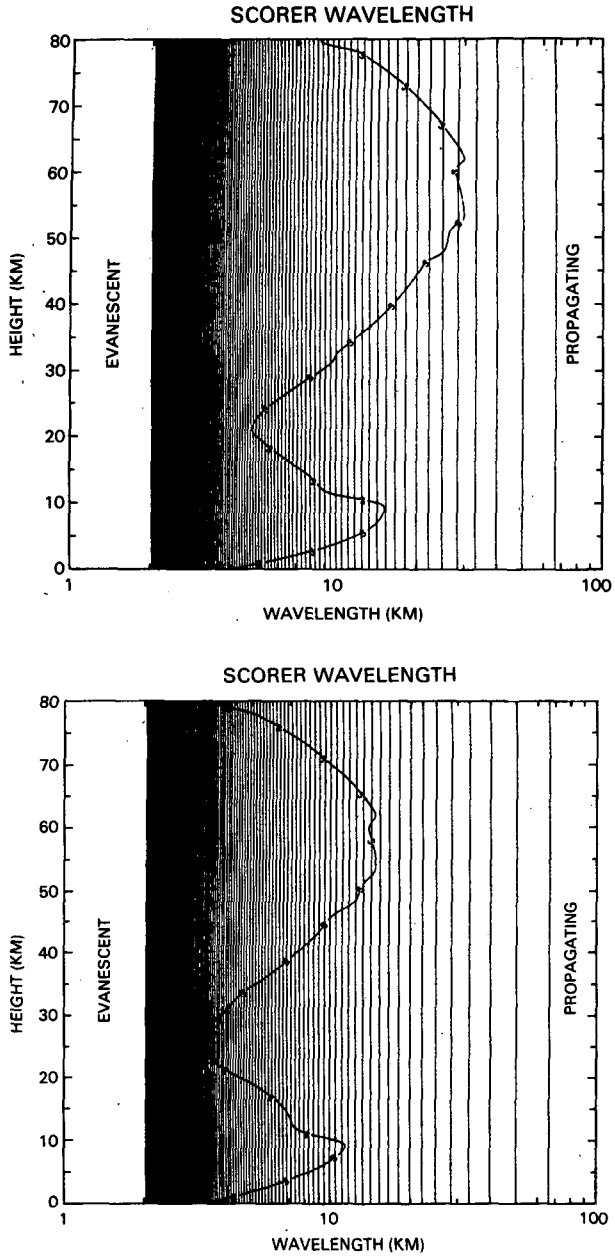

FIG. 3. The various modes of the model with given horizontal wavelength are plotted with the Scorer wavelength ($2\pi/S$). For a particular mode, the intersection of the curve labeled S with the vertical line indicates the altitude of internal reflection. Modes which fall to the left of the $2\pi/S$ curve are evanescent; to the right are propagating. Panels (a) and (b) are for the winter and equinox wind profiles, respectively.

theory) upon which ray tracing is based would no longer be valid]. Table 1 indicates the horizontal wavelength for each ray and the propagation time from the surface to the upper boundary (80 km) or to a reflection level. The wave packet source is near the left boundary.

The refraction of the ray paths which reach the upper boundary coincide quite well with locus of maximum displacement through the stratosphere and mesosphere. The larger downstream shift of the disturbance with altitude for winter relative to that for equinox is due to the stronger zonal flow in the winter profile, and this effect is reflected in the larger refraction of the rays. The transit times shown in Table 1 indicate that the time required to set up a mountain wave pattern like those shown in Fig. 2 would be less than six hours for

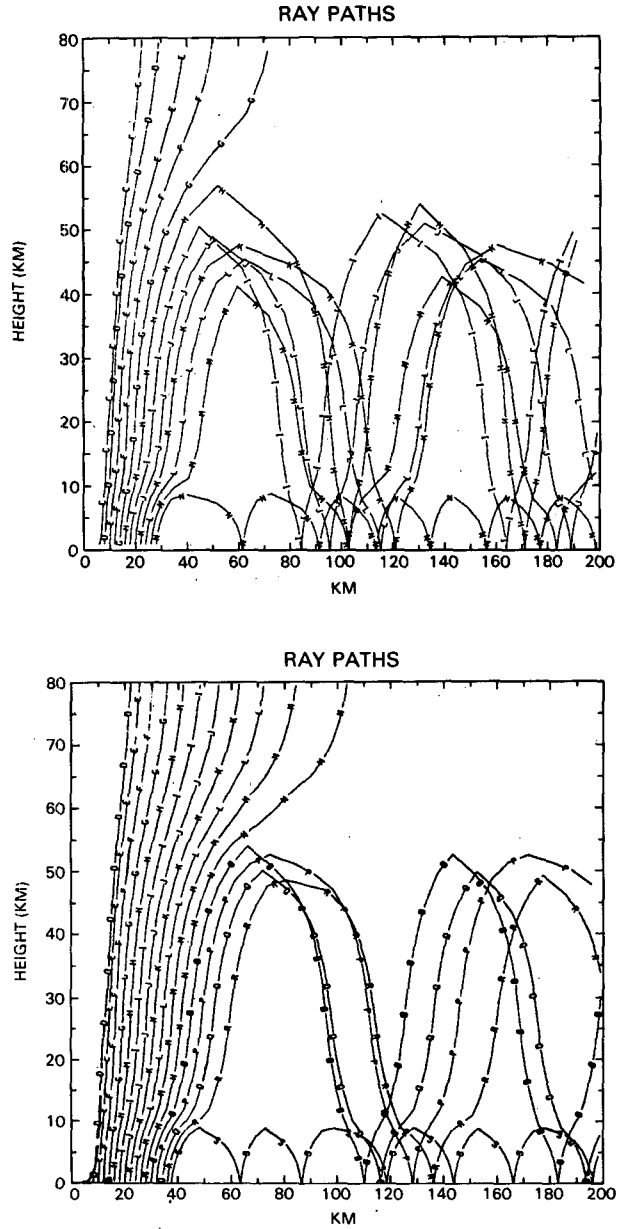

FIG. 4. Ray paths for the longer wavelength modes. The forcing region is near the left boundary and is shifted slightly for each ray path to clarify the figure. Rays which are internally reflected reverse direction. Table 1 gives the corresponding horizontal wavelength for each labeled curve. Panels (a) and (b) correspond to the winter and equinox wind profiles, respectively.

TABLE 1. Transit times for gravity wave packets. Ray labels are given in Fig. 4. The times are the transit times to the reflection level indicated in Fig. 4 or to the upper boundary. The first underline separates rays which have been reflected (below) from those which propagate to 80 km (above). The second line separates those reflected near the stratopause from those reflected near the tropopause.

Ray label	λ_H (km)	Time (hours)	
		Winter*	Equinox†
C	100	7.6	
D	66.6	5.1	13.1
E	50.0	3.8	9.8
F	40.0	3.16	7.94
G	33.3	2.72	6.66
H	28.5	2.2	5.72
I	25.0	1.94	5.0
J	22.2	1.77	4.55
K	20.0	1.61	4.16
L	18.2	1.5	3.8
M	16.6	1.4	3.61
N	15.4	0.44	3.5
O	14.3		2.6
P	13.3		2.5
Q	12.5		2.38
R	11.7		2.33
S	11.1		0.61

* Figure 4a.
† Figure 4b.

the equinox profile and as short as three hours for winter.

A quantitative measure of how far downstream the mountain wave might appear can be estimated by the slope of the ray. From (3),

$$\frac{\Delta z}{\Delta x} = \frac{N}{k\bar{u}}\left(1 - \frac{k^2\bar{u}^2}{N^2}\right)^{1/2}. \quad (4)$$

It is clear from this equation that the ray tilts more to the horizontal for stronger zonal wind profiles and shorter horizontal wavelengths. This is consistent with the results shown in Fig. 4. Comparing Figs. 2 and 4 it is clear that the disturbances upstream of the mountain result from the periodic boundaries.

The stratospheric wave breakdown regions in Fig. 2 are located only above the mountain where the vertical displacements are large. These regions result from wave superposition; that is, no single harmonic has reached wave breaking amplitude, but the combined wave disturbance from all modes is large enough to produce an unstable region. In the mesosphere, aside from the fact that the unstable regions are much larger in scale, individual modes have reached breaking amplitudes.

b. *Hydrostatic solutions*

Hydrostatic solutions to the mountain wave problem are obtained by using Eq. (2). Figure 5 shows the equivalent hydrostatic solution for the equinoctial wind profile which should be compared to Fig. 2b. There are two important differences between the hydrostatic solution and the nonhydrostatic solution. First, because there is no reflection of the wave in the hydrostatic case, the disturbance has nearly the same structure at all altitudes. Second, as previously mentioned, the disturbance does not move downstream from the mountain since $C_{gx} = 0$ in the hydrostatic case. Despite these effects, the hydrostatic and nonhydrostatic solutions are very similar in the stratosphere for the equinoctial profile because enough modes penetrate to the stratosphere so that disturbance broadening with height is not significant. In addition, the zonal wind is weak enough in the equinoctial profile that the downstream advection is not large. The differences between the hydrostatic and nonhydrostatic computation are greater in the mesosphere. At these altitudes the accumulated small-scale wave filtering and downstream advection produce a disturbance unlike the hydrostatic solution.

c. *Implications for parameterization schemes*

Small-scale gravity waves cannot be resolved by general circulation model grids, yet their role is critical to the momentum budget of the middle atmosphere. By considering the WKB solution to the hydrostatic Eq. (2) for a single harmonic, Lindzen (1981) has parameterized the vertical momentum flux convergence associated with a convectively unstable wave by assuming that once the wave breakdown condition is met, wave growth with decreasing density would cease. Holton (1982, 1983) extended this parameterization by considering waves with different phase speeds and tested it in a zonal mean model. Schoeberl (1985) has also developed a parameterization scheme similar to Lindzen's but based on the ray tracing of a wave packet.

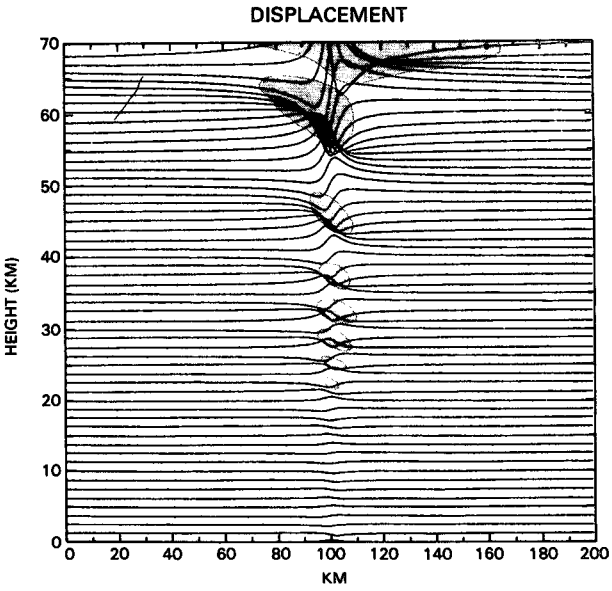

FIG. 5. The particle displacements computed using the hydrostatic Eq. (2) and the equinoctial wind profile. Compare to Fig. 2b.

A fundamental assumption of these parameterization schemes is that gravity wave breakdown occurs for a single characteristic horizontal mode; in other words, the spectrum is monochromatic. From Figs. 2a, b, this assumption is clearly false for the stratosphere. As previously noted, the highly localized nature of the breakdown regions in the stratosphere indicates that no single harmonic has reached breaking amplitude. Instead it is the superposition of stable gravity waves which gives rise to unstable regions. In the mesosphere, however, there is a tendency to monochromaticity as only the largest scale waves are present. This is demonstrated in Fig. 6 where the vertical velocity forcing spectrum is compared with the spectrum at 70 km for both wind profiles. The short horizontal wavelengths have obviously been clipped from the forcing spectrum at 70 km. The spikey sections at shorter wavelengths in Fig. 6 result from decaying resonant modes which have large amplitudes at lower altitudes.

The results shown in Fig. 6 indicate that the vertical velocity spectrum in the mesosphere will peak roughly at the smallest transmitted wavelength if that wavelength is greater than $2\pi a$, the peak in the forcing spectrum for a bell shaped mountain. Thus, there is a tendency to produce a more monochromatic spectrum in the mesosphere through filtering the smaller scale

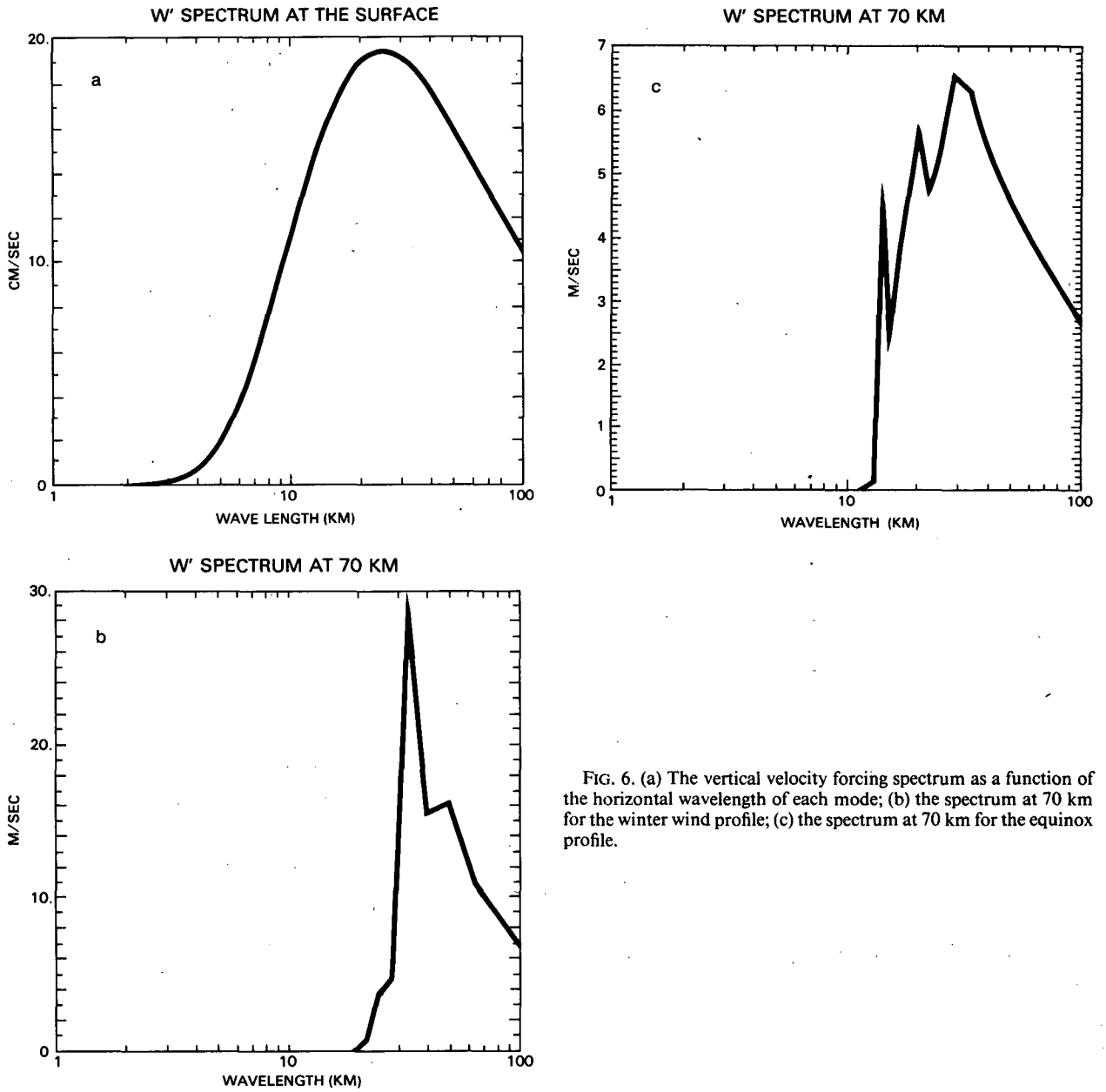

FIG. 6. (a) The vertical velocity forcing spectrum as a function of the horizontal wavelength of each mode; (b) the spectrum at 70 km for the winter wind profile; (c) the spectrum at 70 km for the equinox profile.

modes. However, if the forcing spectrum peak occurs at wavelengths greater than about 30 km the filtering will be less effective in narrowing the spectrum.

We can conclude from these calculations that there is no justification for assuming a monochromatic wavenumber spectrum for stationary gravity waves as is required by Lindzen's (1981) parameterization. This is especially true in the stratosphere where wave superposition is important. In the mesosphere, however, there is a tendency for the spectrum to be narrower because of short wavelength filtering.

Finally, a simple attempt has been made to estimate the momentum flux deposition associated with breaking mountain waves and compare the results with Lindzen's (1981) parameterization. For Lindzen's scheme the wavebreaking formula given by his Eq. (24) was used where $Ri < \frac{1}{4}$ with the effective horizontal wave number approximated by the largest amplitude component of the spectrum. In order to compute the momentum deposition from the model, horizontally independent vertical diffusion was applied in the momentum equation wherever $Ri < \frac{1}{4}$ at some altitude. The model was then iterated adjusting the diffusion until zones with $Ri < \frac{1}{4}$ just disappeared. The vertical momentum flux convergence was then computed.

In every case, the vertical momentum flux convergence estimated using Lindzen's formula was an order of magnitude or more larger than the model results. This occurred because, as previously stated, wavebreaking in the model is principally a result of wave superposition so the wave amplitudes are smaller and the subsequent deceleration is less.

d. Comparison with observations

Vincent and Reid (1983) measured the upward momentum flux phase speeds and horizontal wavelengths of gravity waves over Adelaide using dual beam MST radar. Their observed horizontal wavelength distribution peaks strongly in the 40–80 km range, falling off slowly at higher wavelengths. In the range 0–40 km, however, gravity waves are only 40% as frequent as those in the 40–80 km range. This result appears consistent with the predicted filtering of small scale modes such as shown in Fig. 6.

Another very interesting result from Vincent and Reid is the observed very large spread in horizontal phase speeds of gravity waves. For example, a large number of gravity waves had phase speeds of ± 40 m s^{-1} or greater. Since stationary mountain waves have phase speeds near zero, this result would suggest that most of the observed gravity waves would not arise through topographic forcing. However, one possibility which might explain these observations is the short time scale modulation of mountain waves by flow changes below the mesosphere including fluctuations in the wind flow over the mountain. For example, if the winds at the surface were changing over a few hours, then the amplitude of the mountain wave would pulsate in time which would be interpreted as two gravity waves with opposite phase velocities of the magnitude seen by Vincent and Reid. It should also be noted that there are other rich tropospheric sources of high phase speed gravity waves, namely, jet streaks, organized mesoscale convective activity, frontogenesis and boundary layer instabilities. The short period motion associated with these processes could also contribute to the spectrum of waves observed by Vincent and Reid (1983). The penetration of gravity waves generated by convective activity to the mesosphere has been previously investigated by Clark and Morone (1981).

4. Summary and discussion

The numerical computation of the two-dimensional mountain wave structure up to the mesosphere for equinoctial and winter zonal wind profiles has revealed a number of interesting features. First, there is a general tendency for mountain induced disturbance to broaden in horizontal scale with altitude as smaller-scale modes are filtered with height. The filtering takes place at two distinct altitude regions: the tropopause and the stratopause. These regions locate zones of maximum wind. The selective filtering of gravity with horizontal wavelengths shorter than 30–40 km appears to be consistent with mesospheric gravity wave observations of Vincent and Reid (1983).

Second, the peak vertical displacement in the mesosphere associated with the mountain wave occurs about 40 km downwind of the mountain for the winter zonal wind profile and about 20 km downwind for the equinox profile. This is a nonhydrostatic effect resulting from the existence of a horizontal group velocity. The downstream advection is large enough so that an observer would see no disturbance in the mesosphere directly above the mountain.

Finally, regions of wave instability predicted by this model occur in the stratosphere as a result of wave superposition. That is, each individual harmonic does not reach breaking amplitude, but the sum of the waves produce local regions of instability. In the mesosphere, the unstable regions have a larger horizontal scale because shorter waves are filtered by the intervening atmosphere. From this result it is clear that a monochromatic gravity wave breaking parameterization scheme like Lindzen's (1981) may be more appropriate for the mesosphere than for the troposphere or stratosphere. In the regions where wave superposition is important, monochromatic wave-breaking parameterization will tend to overestimate deceleration.

The computed mountain wave structures have important implications for MST radar programs. Because the radar measures at a fixed site, it cannot distinguish stationary disturbances like mountain waves from the background flow. As a result, the presence of these waves may severely bias the estimates of the large-scale

vertical velocity because of their tendency to appear over the same location. However, several radars whose signals could be correlated spatially may be able to remove this bias. From the results presented here, the separation distance of these radars should be on the order of 20–40 km.

REFERENCES

Bretherton, F. P., 1969: Momentum transport by gravity waves. *Q. J. R. Meteor. Soc.*, **95**, 213–243.

Boer, G. J., N. A. McFarlane, R. Laprise, J. D. Henderson and J.-P. Blanchet, 1984: The Canadian climate centre spectral atmospheric general circulation model, *Atmos. Ocean*, **22**, 397–429.

Clark, J. H. E., and L. T. Morone, 1981: Mesospheric heating due to convectively excited gravity waves—A case study, *Mon. Wea. Rev.*, **109**, 990–1001.

Fels, S. B., 1982: A parameterization of scale dependent radiative damping rates in the middle atmosphere. *J. Atmos. Sci.*, **39**, 1141–1152.

Gill, A. E., 1982: *Atmosphere-Ocean Dynamics*, Academic Press, 662 pp.

Holton, J. R., 1982: The role of gravity wave induced drag and diffusion in the momentum budget of the mesosphere. *J. Atmos. Sci.*, **39**, 791–799.

——, 1983: The influence of gravity wave breaking on the general circulation of the middle atmosphere. *J. Atmos. Sci.*, **40**, 2497–2507.

Klemp, J. B., and D. K. Lilly, 1978: Numerical simulation of hydrostatic mountain waves, *J. Atmos. Sci.*, **35**, 78–107.

——, and ——, 1980: Mountain waves and momentum flux, GARP Publ. No. **23**, 115–141.

Lilly, D. K., 1972: Wave momentum flux—a GARP problem., *Bull. Amer. Meteor. Soc.*, **53**, 17–23.

Lindzen, R. S., 1981: Turbulence and stress due to gravity wave and tidal breakdown. *J. Geophys. Res.*, **86**, 9707–9714.

Matsuno, T., 1982: A quasi one-dimensional model of the middle atmosphere circulation interacting with internal gravity waves. *J. Meteor. Soc. Japan*, **60**, 215–226.

Ogura, Y., and N. A. Phillips, 1962: Scale analysis of deep and shallow convection in the atmosphere, *J. Atmos. Sci.*, **19**, 173–179.

Pierrehumbert, R. T., and B. Wyman, 1985: Upstream effects of mesoscale mountains, submitted to *J. Atmos. Sci.*

Queney, P., 1947: Theory of perturbation in stratified currents with applications to airflow over mountain barriers. Dept. of Meteorology, University of Chicago, Misc. Rep. No. 23.

——, G. A. Corby, N. Gerbier, H. Koschmieder and J. Zierep, 1960: The airflow over mountains, W.M.O. Tech. Note No. 34.

Scorer, R. S., 1949: Theory of lee waves of mountains, *Q. J. R. Meteor. Soc.*, **75**, 41–56.

Schoeberl, M. R., 1985: A ray tracing model of gravity wave propagation and breakdown in the middle atmosphere, submitted to *J. Geophys. Res.*

Smith, R. E., 1979: The influence of mountains in the atmosphere, *Adv. Geophys.*, **21**, 87–230.

Vincent, R. A., and I. M. Reid, 1983: HF doppler measurements of mesospheric gravity wave momentum fluxes. *J. Atmos. Sci.*, **40**, 1321–1333.

Wu, M-F., M. A. Geller, J. G. Olson and M. E. Gelman, 1985: Troposphere–stratosphere (surface–55 km) monthly general circulation statistics for northern hemisphere—four year averages, NASA Tech. Rep. TM 86182, 95 pp.